



2D IR analyses of rate processes in lipid–antibiotic monomolecular films

Saratchandra Shanmukh, Richard A. Dluhy*

Department of Chemistry, University of Georgia, Athens, GA 30602-2556, USA

Received 7 April 2004; received in revised form 3 May 2004; accepted 3 May 2004

Abstract

Polarization modulation infrared reflection spectra of a 1,2-dipalmitoyl-*sn*-glycero-3-phosphatidic acid (DPPA) monolayer on a subphase containing 5 mM tetracycline hydrochloride (TC) were collected under varying surface pressures at the air–water interface. Statistical correlation spectroscopy using 2D IR, $\beta\nu$ and $k\nu$ correlation analyses were performed on these spectra to gain a better understanding of the surface pressure-induced effects on the interaction between the phospholipid and antibiotic. Conventional 2D IR correlation maps revealed strong correlation behavior between the vibrational modes of the lipid and antibiotic. $\beta\nu$ correlation plots provided information about the relative rates of occurrence of the coupled responses noted in the conventional 2D IR plots. These calculations indicated that molecular reorientation occurs at lower surface pressures for the modes in Ring A than for the modes in Ring C. A new model-dependent two-dimensional correlation method, exponential $k\nu$ correlation analysis, confirmed the results from the previous correlation methods and confirmed that the lipid–antibiotic interactions occurred in a bimodal fashion, depending upon surface pressure. The conclusions of the correlation analysis of the surface-pressure induced changes in the DPPA–TC monolayer system lead to the following model for lipid–antibiotic interaction. Initial interaction between the tetracycline molecule and the DPPA molecule occurs at low surface pressures primarily between Ring A of the tetracycline molecule and the lipid headgroup region. However, with increasing surface pressure, the mode of interaction changes, and the strongest interaction at high surface pressures occurs between Ring C of tetracycline and the DPPA headgroup.

© 2004 Published by Elsevier B.V.

Keywords: Infrared spectroscopy; PM-IRRAS; 2D IR correlation spectroscopy; $\beta\nu$ Correlation analysis; $k\nu$ Correlation analysis; Lipid–antibiotic interactions; Monomolecular films

1. Introduction

Two dimensional infrared correlation spectroscopy (2D IR) has proven to be a valuable tool due to its ability to enhance spectral resolution and identify overlapped spectral features [1]. This has proven especially valuable in infrared spectroscopic studies of biomolecules, as this enables one, for example, to identify discrete and unique protein secondary structure conformations as well as interconversion of one form to another as a result of changes in external environment [2–7]. Two-dimensional IR correlation analysis has also been used to analyze structure in monomolecular films.

The phase behavior of phospholipid monolayers have been studied using 2D IR and it was shown how these methods could distinguish bands due to co-existing phases in a disorder-order phase transition in the monolayer [8,9].

Standard 2D IR methods have been most successfully employed in simplifying complex spectra and facilitating band assignments through resolution enhancement [10]. In addition to these uses, 2D IR can also be used to determine the temporal order of events that occur in a set of dynamically varying spectra upon sample perturbation. The basis for this determination is the relative signs of the synchronous and asynchronous cross-peak at coordinate (ν_1, ν_2) in the 2D correlation plots [11].

While it is certainly possible to determine the relative sequence of molecular events based on standard 2D IR methods, this procedure tends to be difficult to implement for highly overlapped spectra and may lead to uncertainties. In order to more quantitatively describe the degree of coherence between spectral intensity changes and the sequence of molecular events in a set of dynamic spectra,

Abbreviations: 2D IR, two-dimensional infrared; A/W, air–water; DPPA, 1,2-dipalmitoyl-*sn*-glycero-3-phosphatidic acid; IRRAS, infrared reflection-absorbance spectroscopy; PEM, photoelastic modulator; PM-IRRAS, polarization modulation–infrared reflectance–absorption spectroscopy; TC, tetracycline hydrochloride

*Corresponding author. Tel.: +1 706 542 1950; fax: +1 706 542 9454.
E-mail address: dluhy@chem.uga.edu (R.A. Dluhy).

we have recently developed a modified 2D IR correlation method called $\beta\nu$ correlation analysis [12]. This method is a variation of asynchronous cross-correlation, in which dynamically varying spectra are correlated against a mathematical function with a varying phase angle. We recently applied $\beta\nu$ correlation analysis to surface pressure-induced changes in the IRRAS spectra of phospholipid monolayers at the A/W interface, and showed how the relative rates of acyl chain and methyl group reorientation could be quantitatively determined [13] and have also applied this analysis in the study of conformational changes and relative reorientation rates of hydrophobic surfactant proteins SP-B and SP-C at the A/W interface [14].

Our current objective is to use polarization-modulation infrared reflection absorption spectroscopy (PM-IRRAS) to study the interactions of the antibiotic tetracycline with a phospholipid monolayer at the air–water interface. It has been shown that tetracycline induces significant changes on phospholipid monolayers and the strongest interactions are observed for the DPPA system due to specific dipole–dipole interactions [15,16]. The aim of the current study is to unambiguously identify the specific regions of interaction between the two molecules at the air–water interface.

To accomplish this aim, we use both conventional 2D IR and $\beta\nu$ correlation analysis to analyze the PM-IRRAS spectra obtained from the lipid–antibiotic interactions. In addition, we introduce a new model-dependent 2D correlation method, $k\nu$ correlation analysis. Our results are able to clearly identify the functional groups involved in this lipid–antibiotic interaction and the order in which their respective functional groups reorient upon increasing monolayer surface pressure.

2. Experimental

2.1. Materials

Tetracycline hydrochloride (TC) was obtained from Sigma (St. Louis, MO, purity > 99%) while 1,2-dipalmitoyl-*sn*-glycero-3-phosphatidic acid (DPPA) (>99%) was

obtained from Avanti Polar Lipids (Alabaster, AL). The chemical structures of tetracycline hydrochloride and DPPA are shown in Fig. 1. HPLC grade chloroform (J.T. Baker, Phillipsburg, NJ) was used as the spreading solvent and typical DPPA concentrations of 1 mg/mL were used for making the spreading solutions. Ultrapure H₂O obtained from a Barnstead (Dubuque, IA) ROpure/Nanopure reverse osmosis/deionization system was used for making the subphase and had a nominal resistivity of 18.3 M Ω cm. The concentration of tetracycline in the subphase was 5 mM.

2.2. PM-IRRAS measurements

Polarization-modulation IR reflection-absorption (PM-IRRAS) measurements at the A/W interface were performed using a Bruker Instruments (Billerica, MA) Equinox 55 Fourier transform infrared spectrometer optically interfaced to a variable angle external reflection accessory (Bruker model XA511-A). The external reflection accessory was equipped with a custom-designed Langmuir trough (Riegler & Kirstein, Berlin, Germany) containing a micro-balance Wilhelmy sensor for surface pressure readings.

PM-IRRAS measurements were performed using previously described protocols [17–20], with changes adapted for our particular experimental design. The IR beam from the interferometer was directed through its external beam port and steered using mirrors into the excitation arm of the reflectance accessory. The excitation arm of the external reflection accessory was rotated using computer-driven stepper motors to achieve an angle of incidence of 74°. Before reflection from the A/W interface, a wire grid polarizer (IGP225, Molectron Detector, Portland, OR) passed *p*-polarized light through a ZnSe photoelastic modulator (PEM-90, Hinds Instruments, Hillsboro, OR) operating at its resonance frequency f_m of 50 kHz. After reflection from the A/W interface, the doubly modulated IR radiation was collected by an *f*/1 ZnSe lens and focused onto the 1 mm² sensing chip of a liquid N₂-cooled photovoltaic

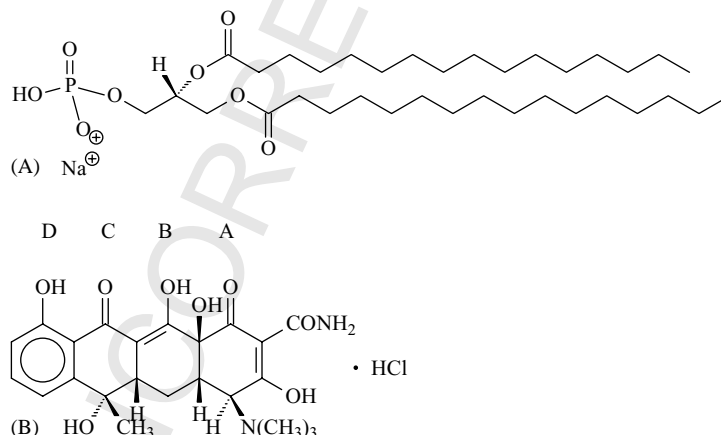


Fig. 1. (A) Structure of 1,2-dipalmitoyl-*sn*-glycero-3-phosphatidic acid (DPPA). (B) Structure of tetracycline hydrochloride (TC). The rings of TC are denoted as indicated in the figure.

HgCdTe detector (KMPV11, Kolmar Technologies, Newburyport, MA). The signal from the HgCdTe detector pre-amplifier may be separated into sum (I_{dc} —resulting from the IR spectrometer) and difference (I_{ac} —resulting from PEM modulation) components using dual-channel electronics with lock-in detection, as previously described [17,19]. PM-IRRAS spectra were recorded at a resolution of 4 cm^{-1} using a scan speed/sampling frequency of 13 kHz. The total acquisition time for each spectrum was 15 min, resulting in 1500 interferograms per spectrum. Further details of the procedure used in our laboratory for collection of PM-IRRAS spectra have been previously reported [21].

2.3. Calculation of 2D IR correlation spectra

The 2D IR synchronous spectrum, $\Phi(v_1, v_2)$ and the asynchronous spectrum, $\Psi(v_1, v_2)$, were calculated as previously described [12,14]. In all cases the average spectrum was subtracted from each sequentially obtained surface pressure-dependent IRRAS spectrum to produce a set of dynamic IR spectra. The resulting dynamic spectra were then used in the correlation analysis.

The 2D plots presented in this article were calculated using 2D IR correlation analysis algorithms written in our laboratory using the MATLAB programming environment (Version 6, The MathWorks, Inc., Natick, MA). These algorithms incorporate the most recent mathematical formalism in which a Hilbert transform is utilized for calculating the asynchronous spectrum rather than the more commonly employed Fourier transform [22].

2.4. PV correlation analysis

A $\beta\nu$ correlation analysis is a mathematical asynchronous cross-correlation performed on a set of dynamically varying IR spectra against a set of sinusoidal functions that differ only by their phase angle β . A full description of the details of the $\beta\nu$ correlation analysis has been presented elsewhere [12], as well as the application of $\beta\nu$ correlation analysis to conformational analysis of monolayer films [13,14]. In this study the $\beta\nu$ correlations were performed with $\phi = 10^\circ$, so that $\sin(k10^\circ + \beta)$ describes approximately 1/4 of the cycle of a sine function, or the approximate form of a commonly observed variation in spectral band intensities upon sample perturbation. Only the asynchronous correlation algorithm is used in the $\beta\nu$ correlation analysis presented here, since asynchronous 2D IR correlations are more sensitive to differences in the form of the signal variation than are synchronous correlations [23].

As previously described, the $\beta\nu$ correlation analysis calculates an effective phase angle, β_e [12]. The effective phase angle β_e is the point of maximum positive correlation intensity in the plot of β versus ν and quantitatively defines the relative rates of reorientation of molecular groups in the set of dynamic spectra.

The $\beta\nu$ plots of effective phase angles versus wavenumber were calculated using $\beta\nu$ correlation analysis algorithms written in our laboratory using the MATLAB programming environment. The computational algorithm for the $\beta\nu$ correlation analysis incorporates the Hilbert transform for calculating the asynchronous spectrum [22].

2.5. Exponential 2D IR correlation— $k\nu$ correlation analysis

A $k\nu$ correlation analysis is a mathematical cross correlation performed between a set of N spectra undergoing some dynamic intensity variation against a set of decreasing exponential functions that are varying in their rate constants [24]. As such, it is a model-dependent 2D IR correlation method analogous to the $\beta\nu$ correlation analysis described above.

A $k\nu$ correlation analysis is mathematically described as shown in Eq. (1). The correlation intensity Ψ at some point (ν, k) represents the correlation of the measured IR spectral intensity $y(\nu, n_j)$ with the mathematical function $\exp(-kt + R)$. In Eq. (1), y is the IR intensity; ν is the frequency or wavenumber; n_j is the number of the spectrum in the ordered sequence where the first spectrum number is zero; k is the rate constant of the exponential curve; N is the total number of spectra used in the calculation; R is a constant matrix, and M_{jk} is the Hilbert–Noda transform matrix previously defined [12,22].

$$\Psi(\nu, k) = \frac{1}{N-1} \sum_{j=0}^{N-1} y(\nu, n_j) \sum_{k=0}^{N-1} M_{jk} \exp(-k + R) \quad (1)$$

The asynchronous $k\nu$ correlation intensity can be either positive or negative depending on the direction and magnitude of intensity change. Based on studies done on simulated spectra, positive peaks are observed when intensities increase and negative peaks are observed when intensities decrease. In the cases of bands where the direction of intensity change varies during the course of the experiment, or when the rate of intensity change decreases, both positive and negative correlation peaks may be observed. A full description of the details of the $k\nu$ correlation analysis has been presented elsewhere [24].

In a $k\nu$ correlation analysis, a new parameter, k_{eff} , is defined from the $k\nu$ correlation plots that is the point of maximum correlation intensity in the plot of k versus ν . The range of values that k_{eff} can take may be arbitrarily set and are between 1 and 7 in this article. The calculated values of k_{eff} are representative of the rates at which the different molecular processes occur. These values are not actual rate constants, per se, but are instead the *relative differences* of the rates defined by the rate constants used in the 2D correlation calculation. As a result, these k_{eff} values are comparable and can be used to assign quantitative rate relationships. Events at spectral frequencies with a larger k_{eff} value occur earlier than events at spectral frequencies at

238 smaller k_{eff} values. Positive and negative k_{eff} values are
 239 comparable and hence no manipulation of the spectra is
 240 required to compare increasing and decreasing bands. As in
 241 the case of the conventional 2D IR correlation analysis,
 242 frequency shifts in band positions affect the shapes of the
 243 correlation peaks observed, however the effects are not as
 244 pronounced. Analysis of simulated frequency-shifted spec-
 245 tral models can identify the cause of the observed frequency
 246 shifting in the correlation plots [8]. In the case of spectral
 247 bands that give both positive and negative correlation peaks
 248 in the $k\nu$ correlation plot, the frequency at which the one
 249 correlation peak occurs would be slightly shifted relative to
 250 the other correlation peak [24].

251 In this current, article, $k\nu$ correlation analyses were
 252 performed on PM-IRRAS spectra of lipid–antibiotic mix-
 253 tures at the A/W interface. Before correlation, the spectra
 254 were normalized for changes in surface density, baseline
 255 corrected using the GRAMS/AI spectral software package
 256 (Galactic, Nashua, NH) and the resulting spectra were
 257 smoothed using a 2nd degree Savitsky–Golay polynomial.
 258 The $k\nu$ plots of effective rate constants versus wavenumber
 259 were calculated using $k\nu$ correlation analysis algorithms
 260 written in our laboratory using the MATLAB programming
 261 environment.

262 3. Results and discussion

263 3.1. Monolayer IR spectroscopy

264 Previous research using monomolecular films of DPPA on
 265 a tetracycline-containing subphase has indicated that spe-
 266 cific inter-molecular interactions may occur between the
 267 polar head groups of the phospholipid in the condensed
 268 phase and the tetracycline molecules dissolved in the sub-
 269 phase [15,16]. In order to test this hypothesis, we employed
 270 polarization-modulation infrared reflectance–absorption
 271 spectroscopy (PM-IRRAS) and obtained IRRAS spectra
 272 at the air–water (A/W) interface for monolayer films of
 273 DPPA on a tetracycline-containing subphase. These lipid–
 274 antibiotic spectra are shown in Fig. 2; the PM-IRRAS
 275 spectra in this figure have been normalized to account for
 276 changes in trough area. Normalization refers to the adjust-
 277 ment of monolayer IR spectral intensities to take into
 278 account changes in surface density as the trough area
 279 available to the monomolecular film decreases during com-
 280 pression. Intensity changes in area-normalized monolayer
 281 spectra more accurately reflect conformational changes in
 282 the monolayer, as apposed to merely reflecting an increase in
 283 number density of molecules in the focus of the IR beam. We
 284 have previously shown that intensity normalization is impor-
 285 tant for understanding 2D IR correlation maps calculated
 286 from IRRAS monolayer spectra [9].

287 The IR spectra presented in Fig. 2 were acquired while the
 288 monolayer was held at specific surface pressure values from
 289 2.0–40.0 mN/m. The main spectral features apparent in the

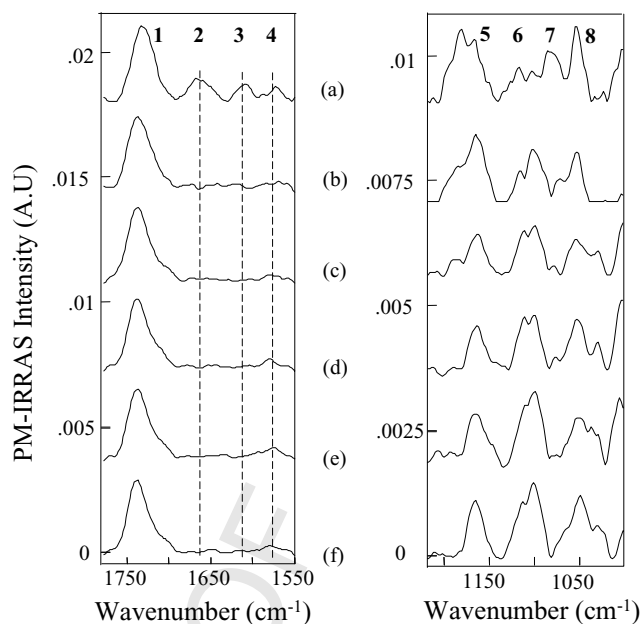


Fig. 2. PM-IRRAS spectra of a DPPA monolayer on a subphase containing 5 mM tetracycline hydrochloride at the air–water interface. The monolayer was applied in organic solution to the A/W interface at low surface pressure. The spectra displayed were acquired at: (a) 3.0 mN/m, (b) 5.0 mN/m, (c) 10.0 mN/m, (d) 20.0 mN/m, (e) 30.0 mN/m, and (f) 40.0 mN/m. In the panel on the left, the band caused by the dispersion of the refractive index of water at $\sim 1640\text{ cm}^{-1}$ has been subtracted out using a fitted Lorentzian curve. The resulting subtracted spectra are presented here. The panel on the right shows the spectral region between 1250 and 1000 cm^{-1} containing: (5) $\nu_{\text{as}}\text{ PO}_4^{2-}$ of DPPA at 1227 cm^{-1} , (6) $\nu_{\text{as}}\text{ C–O–C}$ of DPPA at 1180 cm^{-1} , (7) $\nu_{\text{s}}\text{ PO}_4^{2-}$ of DPPA at 1103 cm^{-1} and (8) $\nu_{\text{s}}\text{ C–O–C}$ of DPPA at 1058 cm^{-1} .

PM-IRRAS spectrum in Fig. 2 are: (1) the C=O band of DPPA at 1737 cm^{-1} , (2) the Amide I mode of the amide group in Ring A of TC at 1660 cm^{-1} , (3) the C=O band in Ring A of TC at 1616 cm^{-1} , and (4) the C=O band in Ring C of TC at 1579 cm^{-1} [15]. As the surface pressure is increased (Fig. 2a–f) the bands at 1660, 1616 and 1579 cm^{-1} rapidly decrease in intensity. This decrease in intensity is attributed to the nature of interaction of the tetracycline molecule present in the subphase with the lipid monolayer. Based on studies of the pressure–area isotherms of this system it has been observed that the greatest degree of insertion occurs at lower surface pressures since the lipid monolayer is less tightly packed [15]. Furthermore, the weak intensities of the tetracycline bands are attributed to the submonolayer nature of the antibiotic interaction with the lipid in which the bulk of the antibiotic molecules are present in the subphase [15].

The panel on the right of Fig. 2 shows the following low-frequency IR bands: (5) the antisymmetric PO_4^{2-} stretching vibration of DPPA at 1227 cm^{-1} , (6) the antisymmetric C–O–C stretching vibration of DPPA at 1180 cm^{-1} , (7) the symmetric PO_4^{2-} stretching vibration of DPPA at

312 1103 cm^{-1} , and (8) the symmetric C–O–C stretching vibra-
 313 tion of DPPA at 1058 cm^{-1} . Two-dimensional IR, $\beta\nu$ and $\nu\nu$
 314 correlation analyses were performed on these PM-IRRAS
 315 spectra to gain a better understanding of the surface pres-
 316 sure-induced effects on the interaction between the phos-
 317 pholipid and antibiotic.

318 3.2. 2D-IR correlation analysis

319 Conventional two-dimensional infrared correlation spec-
 320 troscopy was applied to the dynamic set of PM-IRRAS
 321 DPPA–TC spectra in order to analyze the different spectral
 322 features obtained from the 2D synchronous, $\Phi(\nu_1, \nu_2)$, and
 323 asynchronous, $\Psi(\nu_1, \nu_2)$, maps. The 2D correlation maps
 324 were calculated as previously described [12,14].

325 Fig. 3A shows the 2D synchronous correlation map of the
 326 PM-IRRAS spectra of the DPPA monolayer on the TC
 327 subphase. A strong autopeak is observed at 1737 cm^{-1}
 328 corresponding to the carbonyl stretching vibration due to
 329 the carbonyl group present in the headgroup of the lipid. A
 330 weakly intense autopeak is observed at 1572 cm^{-1} corre-
 331 sponding to the C=O vibration of the carbonyl group present
 332 in Ring C of the TC molecule. A positive cross peak is
 333 observed between 1572 and 1737 cm^{-1} . Positive synchro-
 334 nous cross peaks indicate a coordinated spectral response
 335 in which the functional groups are reorienting in the same
 336 direction. Negative cross peaks are observed at 1657 cm^{-1}
 337 versus 1737 cm^{-1} , 1610 cm^{-1} versus 1737 cm^{-1} and
 338 1572 cm^{-1} versus 1657 cm^{-1} . Negative synchronous cross
 339 peaks indicate significantly coupled molecular reorientation,
 340 albeit one where the spectral intensity of one component
 341 increases while the second decreases. The bands corre-

342 sponding to the amide vibrational mode (1657 cm^{-1}) and
 343 the C=O stretching mode of the carbonyl group in Ring A
 344 (1610 cm^{-1}) of the tetracycline, both give negative peaks
 345 with the carbonyl band of the DPPA molecule, indicating a
 346 coupled (negative) response between the two with respect to
 347 the carbonyl of the phospholipid. The positive cross peak
 348 between the carbonyl group at Ring C and the lipid carbonyl
 349 indicates a different (positive) response from the groups in
 350 Ring A.

351 The asynchronous 2D IR correlation plot of the experi-
 352 mental PM-IRRAS spectra is displayed in Fig. 3B. Asyn-
 353 chronous 2D spectra are antisymmetric with respect to the
 354 diagonal in the correlation map and contain no auto peaks;
 355 the spectrum consists only of off-diagonal cross peaks with
 356 two intensity maxima—one positive and one negative. Peaks
 357 appear in asynchronous 2D correlation maps if the transition
 358 dipole moments are significantly decoupled, or if the dipole
 359 moments reorient out-of-phase or at different rates in
 360 response to the external perturbation. This attribute is used
 361 to unmask the differential response of functional groups in
 362 the molecule, and makes asynchronous 2D correlation plots
 363 particularly useful for resolution enhancement [11]. Promi-
 364 nent cross peaks are observed at 1737 cm^{-1} versus
 365 1761 cm^{-1} (–), 1657 cm^{-1} versus 1737 cm^{-1} (–),
 366 1607 cm^{-1} versus 1737 cm^{-1} (–), 1713 cm^{-1} versus
 367 1735 cm^{-1} (+), 1691 cm^{-1} versus 1735 cm^{-1} (+) and
 368 1574 cm^{-1} versus 1737 cm^{-1} (+).

369 Fig. 4A shows the 2D synchronous correlation map
 370 between the low-frequency region (1250–1020 cm^{-1}) and
 371 the region containing the carbonyl vibrations of the PM-
 372 IRRAS spectra of the DPPA monolayer on the TC subphase.
 373 Since this is a hetero-spectral correlation between different

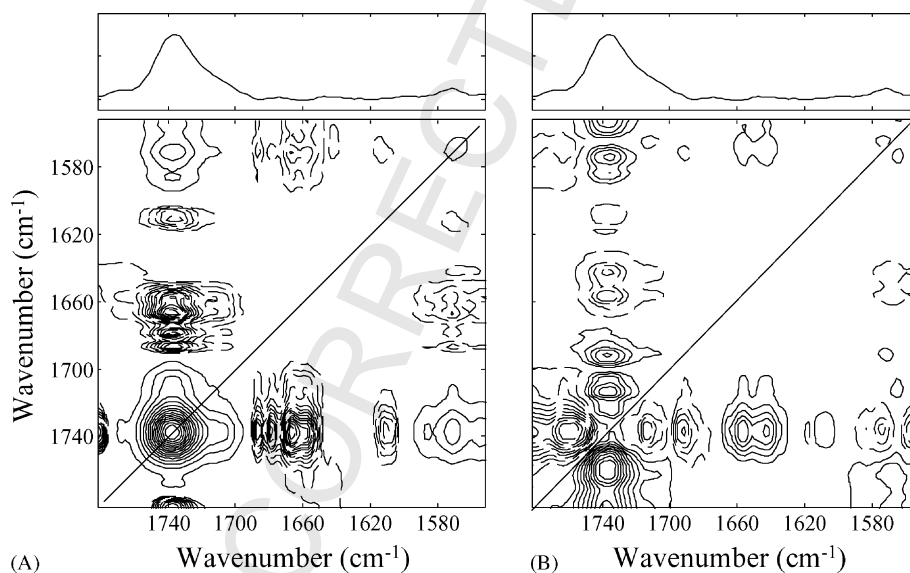


Fig. 3. 2D IR correlation plots of the 1800–1550 cm^{-1} region of the PM-IRRAS spectra of DPPA on the subphase containing 5 mM tetracycline hydrochloride shown in Fig. 2. Solid lines indicate regions of positive correlation intensity, while dashed lines indicate regions of negative correlation intensity. (A) Synchronous 2D correlation plot. (B) Asynchronous 2D correlation plot. In both (A) and (B), the topmost panel illustrates the average spectrum in the dynamic spectral data set used in the correlation calculations.

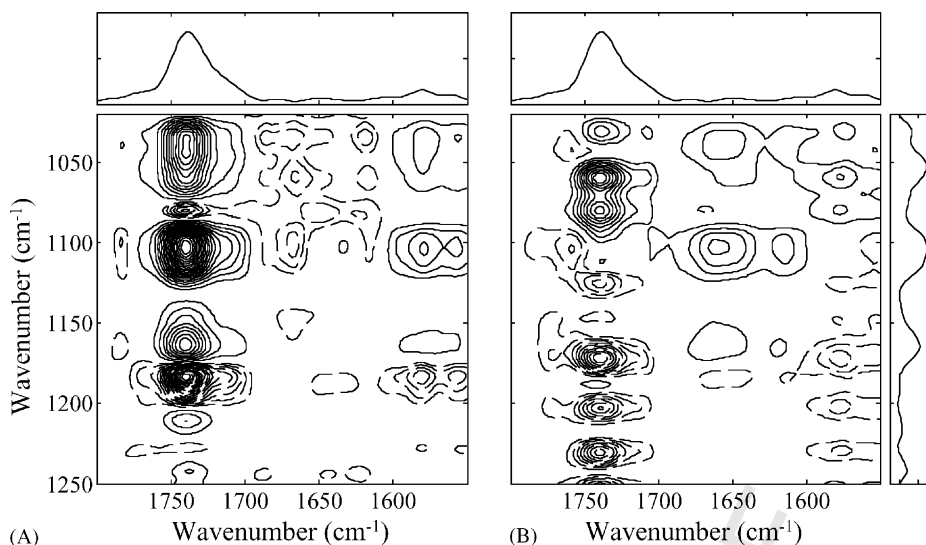


Fig. 4. 2D IR hetero-spectral correlation plots between the regions 1250–1020 and 1800–1550 cm^{-1} . Solid lines indicate regions of positive correlation intensity, while dashed lines indicate regions of negative correlation intensity. (A) Synchronous 2D correlation plot. (B) Asynchronous 2D correlation plot. In both (A) and (B), the topmost panel illustrates the average spectrum in the dynamic spectral data set used in the correlation calculations.

374 regions of the spectrum, no autopeaks will be observed.
 375 Positive cross peaks are observed at 1737 cm^{-1} versus
 376 1048 cm^{-1} , 1737 cm^{-1} versus 1103 cm^{-1} , 1578 cm^{-1} ver-
 377 sus 1048 cm^{-1} and 1578 cm^{-1} versus 1103 cm^{-1} . Negative
 378 cross peaks are observed at 1737 cm^{-1} versus 1184 cm^{-1}
 379 and 1580 cm^{-1} versus 1184 cm^{-1} . The cross peaks due
 380 to the amide band at 1657 cm^{-1} and the carbonyl in Ring
 381 A at 1616 cm^{-1} are very weak in intensity. The presence of
 382 strong cross peaks between the carbonyl ester and phosphate
 383 vibrations with the C=O mode in Ring C (1578 cm^{-1})
 384 indicate a coupled response between these modes. Further-
 385 more, both the C=O of the lipid (1737 cm^{-1}) and the C=O
 386 of Ring C give negative cross peaks with the antisymmetric
 387 ester vibration at 1180 cm^{-1} indicating similar reorientation
 388 behavior of the two carbonyl modes. A close-up of the
 389 region of the map showing the synchronous correlation
 390 between the C=O band in Ring C versus the ester and
 391 PO_4^{2-} vibrations is shown in Fig. 5. It is quite clear from this
 392 plot that there is a strong interaction between Ring C of the
 393 tetracycline molecule and the headgroup region of the
 394 phospholipid.

395 The asynchronous 2D IR correlation plot of the same
 396 region is displayed in Fig. 4B. Prominent cross peaks are
 397 observed at 1737 cm^{-1} versus 1171 cm^{-1} (–), 1737 cm^{-1}
 398 versus 1231 cm^{-1} (–), 1578 cm^{-1} versus 1173 cm^{-1} (–),
 399 1576 cm^{-1} versus 1229 cm^{-1} (–), 1739 cm^{-1} versus
 400 1061 cm^{-1} (+) and 1576 cm^{-1} versus 1059 cm^{-1} (+), while
 401 weak cross peaks are observed at 1658 cm^{-1} versus
 402 1103 cm^{-1} (+) and 1615 cm^{-1} versus 1103 cm^{-1} (+).
 403 The presence of negative peaks between the bands in Ring
 404 A and the symmetric stretch of the PO_4^{2-} group indicates an
 405 out-of-phase behavior between these bands. This will be
 406 discussed further in the sections describing the $\beta\nu$ and $k\nu$
 407 correlation analyses.

3.3. $\beta\nu$ Correlation analysis

408

409 In addition its use in studying structural changes and
 410 making band assignments, 2D IR correlation spectroscopy
 411 has also been used to determine the temporal order of events
 412 that occur during the external sample perturbation. The basis
 413 for this determination is the relative signs of the asyn-
 414 chronous and synchronous cross peaks [11]. A positive asyn-
 415 chronous cross peak at (ν_1, ν_2) indicates that the intensity
 416 change at ν_1 occurs before ν_2 ; a negative cross peak at ν_1 is
 417 observed if the change occurs after ν_2 . This rule, however, is

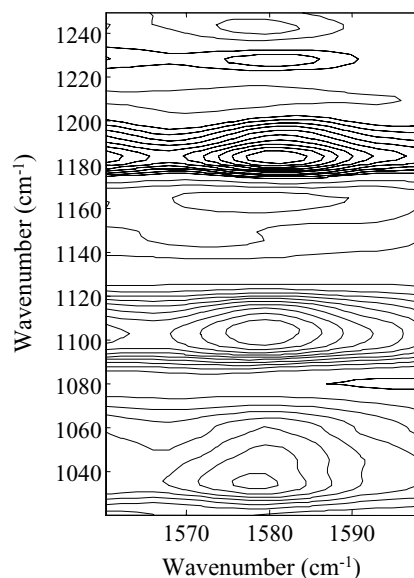


Fig. 5. 2D IR hetero-spectral synchronous correlation plot between the regions 1250–1020 and 1600–1550 cm^{-1} illustrating the cross peaks between the C=O band in Ring C at 1572 cm^{-1} and the phosphate and ester bands in the lipid headgroup region.

418 reversed if the corresponding synchronous peak at (ν_1, ν_2)
 419 has a negative sign, i.e. $\Phi(\nu_1, \nu_2) < 0$. While it is possible to
 420 determine the relative sequence of molecular rearrange-
 421 ments based on comparison of the signs of the cross peaks
 422 in the asynchronous versus synchronous correlation maps,
 423 this procedure is somewhat cumbersome, inherently quali-
 424 tative in nature and leads to uncertainties for highly over-
 425 lapped spectra.

426 In order to more quantitatively describe the degree of
 427 coherence between the observed spectral intensity changes
 428 and the sequence of molecular events in a discrete set of
 429 dynamic spectra, we have developed modified 2D IR meth-
 430 ods that utilize well-known mathematical functional forms
 431 to simulate experimental IR intensity variations. One such
 432 method is $\beta\nu$ correlation analysis, in which an asynchronous
 433 cross-correlation is performed using a set of dynamically
 434 varying spectra, i.e. $y(\nu, n_j)$, against a sine function of the
 435 form $\sin(k\phi + \beta)$ [12].

436 The resulting correlation intensities are a function of the
 437 spectral frequency (ν) and the phase angle (β) of the
 438 mathematical function. The maximum correlation intensity
 439 will be observed at one point (ν, β) in the correlation plot
 440 for the range $360 > \beta > 0$. This point is used to define a new
 441 parameter—the effective phase angle β_e of $f(\nu, \beta)$. The β_e
 442 value quantitatively reveals the degree of coherence between
 443 the experimental intensities and the sequence of molecular
 444 events in a discrete set of dynamic spectra. We recently
 445 applied $\beta\nu$ correlation analysis to surface pressure-induced
 446 changes in the IRRAS spectra of phospholipid monolayers at
 447 the A/W interface, and showed how the relative rates of acyl
 448 chain and methyl group reorientation could be quantitatively
 449 determined [13]. We have also applied this method to
 450 surface pressure induced conformational changes in the

Table 1

Values of the effective phase angle, β_e , obtained from the $\beta\nu$ plots in Figs. 6 and 7

Observed value (cm^{-1})	Assignment	β_e
1737	C=O of DPPA	51.8
1657	Amide group	242.1
1616	C=O of Ring A	240.1
1579	C=O of Ring C	55
1227	Asym. PO_4^{2-}	241.9
1180	Asym. C–O–C	241.1
1103	Sym. PO_4^{2-}	51.7
1058	Sym. C–O–C	62.3

secondary structure of hydrophobic surfactant proteins 451
 SP-B and SP-C at the air–water interface [14]. 452

453 We have applied $\beta\nu$ correlation analysis to the PM-IRRAS 453
 spectra of the DPPA monolayer on the tetracycline contain- 454
 ing subphase. The $\beta\nu$ correlation plot for of these spectra is 455
 shown in Fig. 6. In addition, the values for the effective 456
 phase angle (β_e) and the band assignments for the peaks in 457
 this plot are presented in Table 1. It is immediately obvious 458
 from Fig. 6 that the most intense peak in the $\beta\nu$ plot is 459
 observed at 1737 cm^{-1} corresponding to the carbonyl group 460
 in the phospholipid headgroup. Peaks at 1657, 1616 and 461
 1579 cm^{-1} corresponding to the Amide band in Ring A, 462
 C=O group in Ring A and the C=O group in Ring C of the 463
 tetracycline molecule, respectively. From the β_e values in 464
 Table 1, it is apparent that there are two distinct groups of β_e 465
 values. The modes in Ring A have β_e values of 242.1 and 466
 240.1, while the C=O mode in Ring C has a β_e value of 55.0, 467
 indicating that the vibrational modes attributed to Ring A 468
 reorient simultaneously and earlier than do the modes from 469
 Ring C. The presence of peaks at these wavenumber values 470

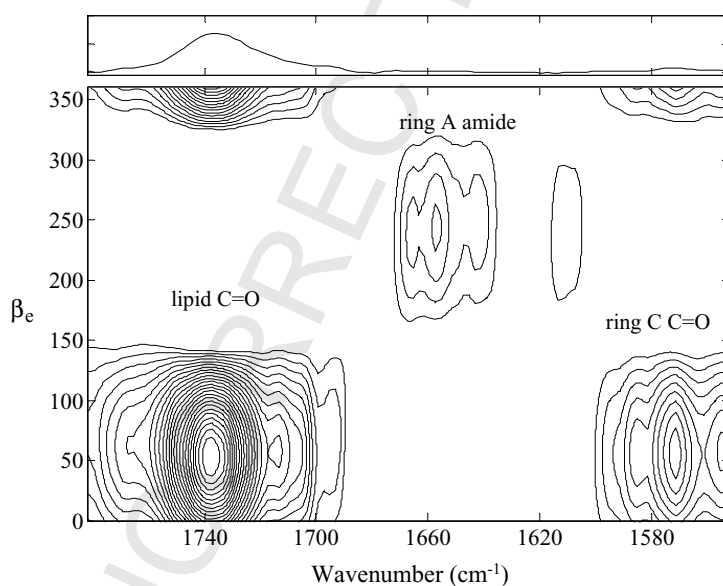


Fig. 6. 2D $\beta\nu$ phase angle correlation plots calculated in the $1800\text{--}1550 \text{ cm}^{-1}$ region of the monolayer PM-IRRAS spectra of DPPA on the subphase containing 5 mM tetracycline hydrochloride shown in Fig. 2. The topmost panel illustrates the average spectrum in the dynamic spectral data set used in the correlation calculations.

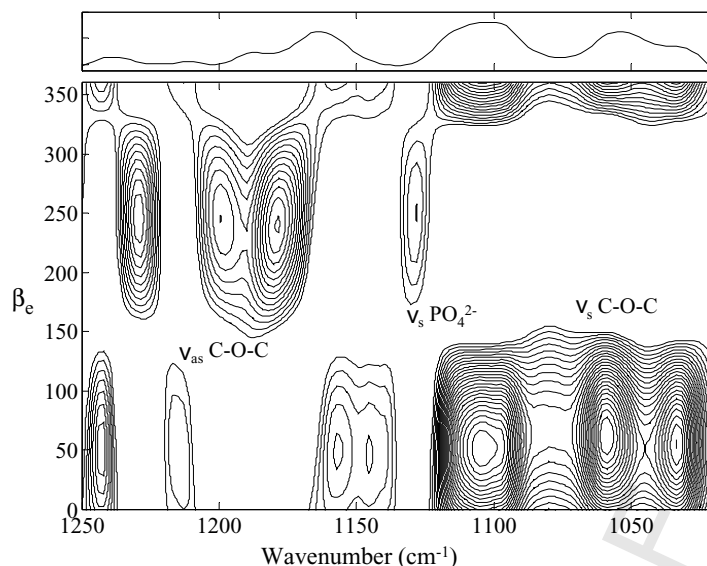


Fig. 7. 2D $\beta\nu$ phase angle correlation plots calculated in the region 1250–1020 cm^{-1} using the monolayer PM-IRRAS spectra of DPPA/5 mM tetracycline hydrochloride shown in Fig. 2. The topmost panel illustrates the average spectrum in the dynamic spectral data set used in the correlation calculations.

471 also confirms their presence in the 2D-IR synchronous and
472 asynchronous maps.

473 $\beta\nu$ Correlation analysis was also applied to the region of
474 the PM-IRRAS spectra containing the vibrations of the
475 headgroup carbonyl ester and phosphate groups (1250–
476 1020 cm^{-1}); this correlation plot is displayed in Fig. 7. In
477 addition, the values for the effective phase angle (β_e) and
478 the band assignments for the peaks in this plot are included
479 in Table 1. Intense peaks in the $\beta\nu$ plot are observed
480 at 1227 cm^{-1} , due to the asymmetric PO_4^{2-} stretch,
481 1180 cm^{-1} , corresponding to the antisymmetric stretch of
482 the carbonyl esters, 1103 cm^{-1} , due to the symmetric stretch
483 of the PO_4^{2-} group and at 1058 cm^{-1} corresponding to the
484 symmetric carbonyl ester stretching vibration. From the β_e
485 values in Table 1, it is apparent that the symmetric stretching
486 modes of the ester (51.7) and the phosphate group (62.3)
487 have similar β_e values to the C=O group in the lipid (51.8)
488 and the C=O group in Ring C (55), indicating a similar
489 reorientation response to increasing monolayer surface pres-
490 sure. The asymmetric stretching modes of the C–O–C and
491 PO_4^{2-} groups have similar β_e values (241.9 and 241.1,
492 respectively) to the amide I and C=O vibrations of Ring
493 A (242.1 and 240.1), indicating a simultaneous reorientation
494 of this portion of the lipid along with this region of the
495 antibiotic that occurs early in the monolayer compression.

496 3.4. $k\nu$ Correlation analysis

497 We have also investigated the suitability of additional
498 mathematical functions for use in model-dependent 2D IR
499 correlation analysis. This article describes the application of
500 one such function, i.e. an exponential function, as a math-
501 ematical waveform that simulates IR intensity variations.
502 We have calculated the asynchronous correlations between
503 the dynamically varying experimental PM-IRRAS spectra

and a simulated exponential data set of the form
471 $\exp(-kt + R)$. The resulting correlation intensities are a
472 function of the spectral frequency (ν) and the rate constant
473 (k) of the exponential function. A maximum or minimum
474 correlation intensity will be observed at one point (ν, k) in
475 the correlation plot. A new parameter, k_{eff} , is defined from
476 the $k\nu$ correlation plots that is the point of maximum
477 correlation intensity in the plot of k versus ν . Both positive
478 and negative correlation intensities are plotted since they
479 represent the differences in the rate of intensity change of
480 individual spectral bands from those of the exponential
481 curves used in the correlation. Correlation maxima are
482 observed at a point ($\nu, k+$) when there is an increase in
483 the infrared intensity in the positive direction and correlation
484 minima are observed at ($\nu, k-$) when there is an increase in
485 the intensity in the negative direction. The ' k ' values quan-
486 titatively reveal the degree of coherence between the experi-
487 mental intensities and the sequence of molecular events in a
488 discrete set of dynamic spectra. Since positive and negative
489 ' k ' values can be directly compared, assignment of the event
490 sequence can be achieved intuitively, and without any
491 modification to the correlation results. Application of this
492 correlation method to models of simulated IR spectra has
493 shown that this is indeed a robust method and can be used to
494 deduce quantitative temporal relationships between molec-
495 ular events. A detailed description of this technique will be
496 presented elsewhere.

507 We have applied the $k\nu$ exponential correlation analysis
508 method to the PM-IRRAS spectra of the DPPA monolayer
509 on the subphase containing tetracycline. The $k\nu$ correlation
510 plots for this system are shown in Figs. 8 and 9. The upper
511 panel represents the region of positive correlation intensity
512 and the lower panel represents the region of negative correla-
513 tion intensity. The values for the effective rate constant
514 (k_{eff}) and the respective band assignments are presented in

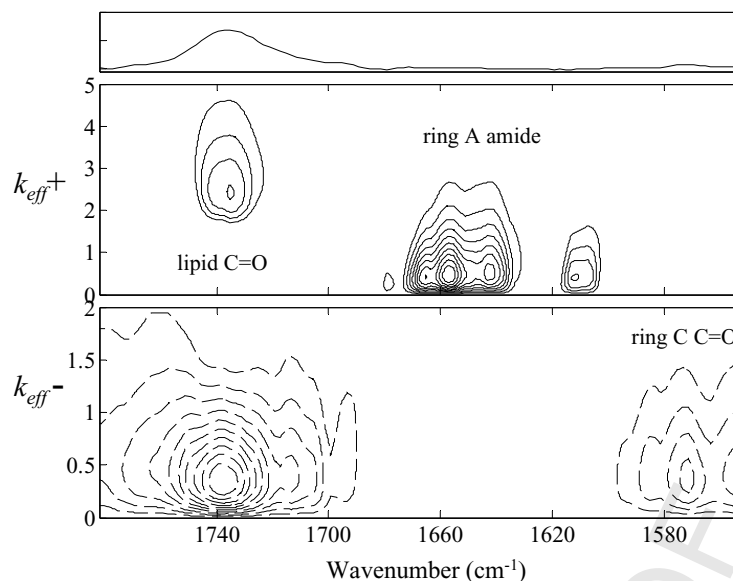


Fig. 8. 2D kv Exponential correlation plots calculated in the region $1800\text{--}1550\text{ cm}^{-1}$ using the monolayer PM-IRRAS spectra of DPPA/5 mM tetracycline hydrochloride shown in Fig. 2. The topmost panel illustrates the average spectrum in the dynamic spectral data set used in the correlation calculations. The center panel illustrates positive kv correlation intensities (i.e. $k_{\text{eff}+}$), while the lower panel illustrates negative kv correlation intensities (i.e. $k_{\text{eff}-}$).

539 Table 2. For the high frequency region, the kv correlation
 540 maps reveal peaks at 1736 , 1657 , 1616 and 1579 cm^{-1}
 541 (Fig. 8). The correlation peaks observed in the kv plot
 542 (Table 2) are identical to those observed in the $\beta\nu$ correlation
 543 plots (Table 1).

544 Based on the signs of the correlation peaks and the values
 545 of the effective rate constants the following inferences can
 546 be made. It is immediately apparent from Fig. 8 that the band
 547 at 1736 cm^{-1} , due to the lipid carbonyl group, has both
 548 positive and negative correlation peaks. Since the $k_{\text{eff}+}$

549 value of the 1736 cm^{-1} peak (2.44), is significantly larger
 550 than the $k_{\text{eff}-}$ value (-0.36), it can be concluded that the
 551 intensity of the carbonyl group increases substantially as the
 552 monolayer is initially compressed. However, as the mono-
 553 layer reaches higher surface pressures, the rate of intensity
 554 increase declines. Since dipole moments reorienting simi-
 555 larly have the same sign for the correlation intensity, it can
 556 be said that the bands due to Ring A of the TC molecule at
 557 1616 cm^{-1} ($k_{\text{eff}+} = 0.41$) and 1657 cm^{-1} ($k_{\text{eff}+} = 0.48$)
 558 reorient similarly at nearly identical rates. The band at

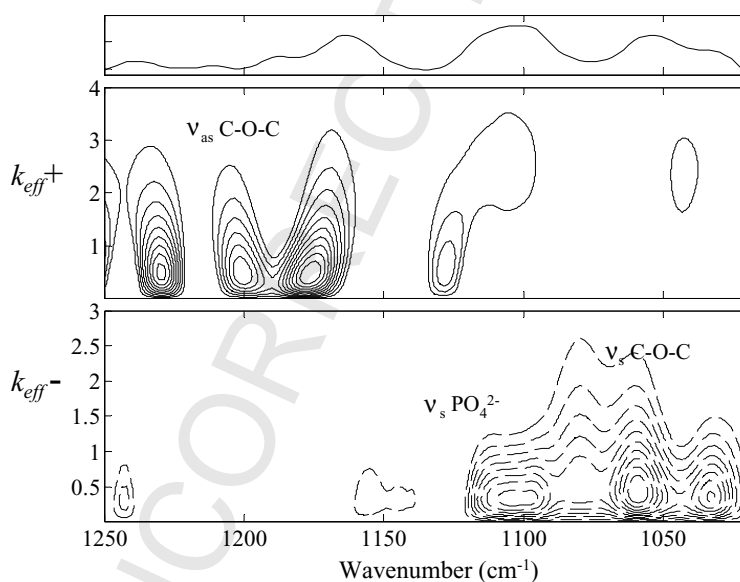


Fig. 9. 2D kv Exponential correlation plots calculated in the region $1250\text{--}1020\text{ cm}^{-1}$ using the monolayer PM-IRRAS spectra of DPPA/5 mM tetracycline hydrochloride shown in Fig. 2. The topmost panel illustrates the average spectrum in the dynamic spectral data set used in the correlation calculations. The center panel illustrates positive kv correlation intensities (i.e. $k_{\text{eff}+}$), while the lower panel illustrates negative kv correlation intensities (i.e. $k_{\text{eff}-}$).

Table 2

Values of the effective rate constants, $k_{\text{eff}+}$ and $k_{\text{eff}-}$ obtained from the $k\nu$ plots in Figs. 8 and 9

Observed value (cm^{-1})	Assignment	$k_{\text{eff}+}$	$k_{\text{eff}-}$
1737	C=O of DPPA	2.44	0.36
1657	Amide group	0.48	–
1616	C=O of Ring A	0.41	–
1579	C=O of Ring C	–	0.36
1227	Asym. PO_4^{2-}	0.49	–
1180	Asym. C–O–C	0.47	–
1103	Sym. PO_4^{2-}	–	0.30
1058	Sym. C–O–C	–	0.41

559 1572 cm^{-1} , corresponding to the C=O in Ring C, has a
560 negative correlation peak at ($k_{\text{eff}-} = -0.37$), indicating a
561 substantially different reorientation behavior than the groups
562 in Ring A.

563 We have also applied $k\nu$ exponential correlation analysis
564 to the low-frequency region of the PM-IRRAS spectra
565 containing the bands due to the phosphate and carbonyl
566 ester groups in the lipid headgroup (1250–1000 cm^{-1}). The
567 $k\nu$ correlation plot is shown in Fig. 9; the calculated values
568 for the effective rate constant (k_{eff}) and the respective band
569 assignments are presented in Table 2. The $k\nu$ correlation
570 maps reveal peaks at 1227, 1180, 1103 and 1058 cm^{-1}
571 (Fig. 9). Using arguments similar to those discussed above,
572 Fig. 9 indicates that the PO_4^{2-} group ($k_{\text{eff}+} = 0.49$) and the
573 carbonyl ester ($k_{\text{eff}+} = 0.47$) reorient at nearly identical
574 rates. It is apparent from Table 2 that these k_{eff} values are
575 similar to the k_{eff} values for the modes in Ring A, indicating
576 a similar rate of reorientation. From Fig. 9, it is observed
577 that the correlation peaks due to the symmetric stretches
578 of the PO_4^{2-} group and the carbonyl esters at 1103 cm^{-1}
579 ($k_{\text{eff}-} = -0.3$) and 1058 cm^{-1} ($k_{\text{eff}-} = -0.41$) respec-
580 tively have similar k_{eff} values. These k_{eff} values are almost
581 identical to those of the C=O band present in Ring C of the
582 tetracycline molecule ($k_{\text{eff}-} = -0.37$) and the C=O band of
583 the lipid at higher pressures ($k_{\text{eff}-} = -0.36$). It can be
584 concluded based on the signs and the values of the k_{eff}
585 values that the symmetric stretching modes of the phosphate
586 and the ester groups in the lipid headgroup have a strong
587 interaction with the Ring C carbonyl mode and reorient at a
588 similar rate.

589 We propose the following conclusions based on the k_{eff}
590 values taken from the $k\nu$ correlation plots of the DPPA–TC
591 monolayer. Previous studies have postulated a specific
592 “electrostatic” interaction between the tetracycline mole-
593 cule and the head group of phospholipids and that this
594 interaction is most significant for the acid head group in
595 DPPA [16]. Previous UV–vis and FTIR/ATR spectra sug-
596 gested intermolecular interactions occur between the TC
597 amide group and DPPA [15]. From the current study, the β_c
598 and k_{eff} values demonstrate that the molecular groups in
599 Ring A of the TC molecule undergo reorientational changes
600 at identical rates and in the same direction as does the DPPA
601 headgroup carbonyl. These data indicate a specific inter-

602 molecular interaction between Ring A of the tetracycline
603 and the headgroup of the phospholipid occurs at low surface
604 pressures. However, at higher surface pressures, reorienta-
605 tion of the carbonyl group of Ring C occurs in concert with
606 the lipid carbonyl and headgroups. Therefore, Region C of
607 the antibiotic interacts more strongly with the lipid at high
608 surface pressures.

4. Conclusions 609

610 Polarization modulation infrared reflection spectra of a
611 dipalmitoyl phosphatidic acid monolayer on a subphase
612 containing 5 mM tetracycline hydrochloride were collected
613 under varying surface pressures. Two-dimensional IR, $\beta\nu$
614 and $k\nu$ correlation analyses were performed on these PM-
615 IRRAS spectra to gain a better understanding of the surface
616 pressure-induced effects on the interaction between the
617 phospholipid and antibiotic.

618 The synchronous 2D IR correlation map reveal strong
619 correlation behavior between the C=O of the DPPA, the
620 amide and C=O mode of Ring A, the C=O mode of Ring C,
621 as well additional lipid headgroup modes (Figs. 3–5). The
622 presence of cross peaks in the synchronous correlation
623 indicates the presence of a coupled response in the reor-
624 ientation of the dipole moments of the modes from the lipid
625 and antibiotic, but complete information about how that
626 reorientation occurs is not available.

627 The $\beta\nu$ correlation plots (Figs. 6 and 7) help to provide
628 information about the relative rates of occurrence of the
629 coupled responses noted in the conventional 2D IR plots.
630 From the β_c values of the different correlation peaks listed in
631 Table 1, it can be seen that the peaks due to the bands in Ring
632 A have a greater β_c value than either the peaks due to the
633 carbonyl in Ring C or the peak due to the lipid carbonyl
634 band. This indicates that the reorientation occurs earlier for
635 the modes in Ring A, i.e. at lower pressures, than the mode in
636 Ring C. This is also supported by the rapid decrease in
637 intensity of the absorption bands corresponding to the amide
638 group and the carbonyl in Ring A in the one-dimensional
639 PM-IRRAS spectrum, as the surface pressure of the mono-
640 layer is increased.

641 A new model-dependent two-dimensional correlation
642 method, exponential $k\nu$ correlation analysis, provided
643 further insights into the rates of reorganization of different
644 monolayer components upon increasing surface pressure
645 (Figs. 8 and 9). For example, the lipid carbonyl band at
646 1736 cm^{-1} shows both positive and negative values for its
647 effective rate constant, k_{eff} . The bimodal distribution of the
648 k_{eff} value for the 1736 cm^{-1} band is reflected in the vibra-
649 tional modes arising from the tetracycline antibiotic. First,
650 the amide I vibration and the C=O vibration from Ring A of
651 the TC molecule both have positive k_{eff} values nearly
652 identical to several lipid headgroup bands. This relationship
653 is also revealed in the $\beta\nu$ correlation plots, indicating that the
654 Ring A vibrational modes reorient early and in concert with

phospholipid headgroup. Secondly, the C=O vibration from Ring C of the TC molecule has a negative k_{eff} value identical to that of the lipid carbonyl band. These data indicate there is a strong interaction between the lipid and antibiotic and that they reorient simultaneously at high surface pressures.

A consideration of the 2DIR correlation analysis of the surface-pressure induced changes in the DPPA–TC monolayer system leads to the following model for lipid–antibiotic interaction. Initial interaction between the tetracycline molecule and the DPPA molecule occurs at low surface pressures primarily between Ring A of the tetracycline molecule and the lipid headgroup region. However, with increasing surface pressure, the mode of interaction changes, and the strongest inter-molecular interactions at high surface pressures occurs between Ring C of tetracycline and the DPPA headgroup.

Acknowledgements

The work described here was supported by the US Public Health Service through National Institutes of Health grant EB001956 (R.A.D.).

References

- [1] I. Noda, A.E. Dowrey, C. Marcott, G.M. Story, Y. Ozaki, *Appl. Spectrosc.* 54 (2000) 236.
- [2] A. Filosa, Y. Wang, A.A. Ismail, A.M. English, *Biochemistry* 40 (2001) 8256.
- [3] M.-J. Paquet, M. Laviolette, M. Pezolet, M. Auger, *Biophys. J.* 81 (2001) 305.
- [4] C.P. Schultz, O. Barzu, H.H. Mantsch, *Appl. Spectrosc.* 54 (2000) 931.
- [5] N. Sefara, N.P. Magtoto, H.H. Richardson, *Appl. Spectrosc.* 51 (1997) 536.
- [6] F. Ismoyo, Y. Wang, A.A. Ismail, *Appl. Spectrosc.* 54 (2000) 939.
- [7] D.K. Graff, B. Pastrana-Rios, S.Y. Venyaminov, F.G. Prendergast, *J. Am. Chem. Soc.* 119 (1997) 11282.
- [8] D.L. Elmore, R.A. Dluhy, *Colloids Surf. A* 171 (2000) 225.
- [9] D.L. Elmore, R.A. Dluhy, *Appl. Spectrosc.* 54 (2000) 956.
- [10] Y. Ozaki, I. Noda (Eds.), *Two-Dimensional Correlation Spectroscopy*, American Institute of Physics, New York, 2000.
- [11] I. Noda, *Appl. Spectrosc.* 47 (1993) 1329.
- [12] D.L. Elmore, R.A. Dluhy, *J. Phys. Chem. B* 105 (2001) 11377.
- [13] D.L. Elmore, S. Shanmukh, R.A. Dluhy, *J. Phys. Chem. A* 106 (2002) 3420.
- [14] S. Shanmukh, P. Howell, J.E. Baatz, R.A. Dluhy, *Biophys. J.* 83 (2002) 2126.
- [15] G. Caminati, C. Focardi, G. Gabrielli, F. Gambinossi, B. Mecheri, M. Nocentini, M. Puggelli, *Mat. Sci. Eng. C* 22 (2002) 301.
- [16] F. Gambinossi, B. Mecheri, G. Caminati, M. Nocentini, M. Puggelli, G. Gabrielli, *Mat. Sci. Eng. C* 22 (2002) 283.
- [17] D. Blaudez, T. Buffeteau, J.C. Cornut, B. Desbat, N. Escafre, M. Pezolet, J.M. Turllet, *Appl. Spectrosc.* 47 (1993) 869.
- [18] D. Blaudez, J.-M. Turllet, J. Dufourcq, D. Bard, T. Buffeteau, B. Desbat, *J. Chem. Soc., Faraday Trans.* 92 (1996) 525.
- [19] T. Buffeteau, M. Pezolet, *Appl. Spectrosc.* 50 (1996) 948.
- [20] T. Buffeteau, B. Desbat, M. Pezolet, J.M. Turllet, *J. Chim. Phys. Phys. Chim. Biol.* 90 (1993) 1467.
- [21] R.A. Dluhy, S. Shanmukh, J.B. Leopard, P. Krieger, J.E. Baatz, *Biophys. J.* 85 (2003) 2417.
- [22] I. Noda, *Appl. Spectrosc.* 54 (2000) 994.
- [23] I. Noda, *Appl. Spectrosc.* 44 (1990) 550.
- [24] S. Shanmukh, R.A. Dluhy, *J. Phys. Chem. A* (2004), in press.

UNCORRECTED